Available online at www.sciencedirect.com
SCIENCE DIRECT®
Journal of the European Ceramic Society 25 (2005) 2627–2632
www.elsevier.com/locate/jeurceramsoc

Modeling and experimental validation of solid oxide fuel cell materials and stacks

J. Van herle *, D. Larrain, N. Autissier, Z. Wuillemin, M. Molinelli, D. Favrat

Laboratory for Industrial Energy Systems (LENI), Faculty of Engineering (STI), Swiss Federal Institute of Technology (EPFL), CH-1015 Lausanne, Switzerland

Available online 20 April 2005

Abstract

Results on solid oxide fuel cell stacks tested at 800 °C with H_2 fuel and using planar Ni-zirconia anode supported cells, 80 mm × 80 mm × 0.2 mm in size, are presented. Modeling and numerical simulation is used to interpret observed results and develop improved designs. Where necessary, the models are calibrated with additional experimental data. Emphasis is placed on the critical issue of nickel anode reoxidation, related to the fuel flow field. Consideration is also given to gradients of temperature und current density developing over the cells and predicted by the models; local current density could be validated by measurement. Flow distribution within stacks is also illustrated by both experimental and modeling results.

Keywords: Fuel cells; Transition metal oxide; Composites; Failure analysis; Flow field

1. Introduction

A promising design in solid oxide fuel cell research is the one using the anode as mechanical supporting structure,[1] normally a porous composite of nickel and zirconia particles. It allows to be made thin (0.2 mm)[2] and cofired using mass production techniques such as tape casting[2] with a thin zirconia electrolyte operating at temperatures around 800 °C, with advantages in cost (for metal interconnect and housing) and lifetime (degradation rates are lowered when reducing operating temperature). The porous thin Ni-zirconia anode support structure, under anodic polarisation with steam production, poses the challenge of operational stability, owing to the presence of thermal gradients and of the Ni-NiO equilibrium. This certainly applies to larger area cells packed in stacks where fuel flow fields develop within the limits given by the cell configuration and boundary conditions, leading to fuel depletion and thermal constraint. To achieve reliable and sufficient electrical output from such cells, experimentation goes in pair with modeling in order to explain and predict results, and to give input to improved design. This contribution presents our development on tape cast Ni anode supported cells, from the experimental observation and modeling points of view, with emphasis on the flow fields in cells and stacks.

2. Experimental

Fabrication of the materials, cells and stacks has been reported in more detail before.[3] The Ni-zirconia anode supports are made from powder mixtures of NiO (in house or J.T. Baker) and 8 mol% yttria-stabilized zirconia (Tosoh). Aqueous tape casting followed by drying, punching and sintering (together with an 8YSZ electrolyte, 5 μm thin) produces square cells of 80 mm × 80 mm × 0.2 mm with one hole each for fuel and air supply as inlets (decentralised, on the symmetry axis) and featuring distributed outlets (slots on the cell edge opposite to the supply hole).[4] The sintered samples are stacked in SOFCONNEX™ design[3] with sheet metal iron–chromium interconnects, and tested in electrical furnaces at around 800 °C with H_2 fuel and air.[3] Airflow is defined with respect to fuel flow by its λ-value, $\lambda_{air} = 1$ being

* Corresponding author. Tel.: +41 21 6933510; fax: +41 21 6933502.
E-mail address: Jan.Vanherle@epfl.ch (J. Van herle).

0955-2219/$ – see front matter © 2005 Elsevier Ltd. All rights reserved.
doi:10.1016/j.jeurceramsoc.2005.03.225

equal to stoichiometry. The active area is 50 cm^2 and the height of anode and cathode gas circulation zones 0.5–1 mm.

Numerical simulation is carried out using computational fluid dynamics, CFD (FLUENT^{TM} 6.0), and the gPROMS equation solver package.[5]

3. Results and discussion

3.1. Anode flow field and nickel stability

The Ni-NiO equilibrium condition with respect to temperature and oxygen partial pressure, crucial to the fuel cell anode operation, is plotted in Fig. 1. At 800 °C, equilibrium PO_2 is equal to 1.2×10^{-14} atm, corresponding to a cathode–anode potential difference of 0.704 V. Nernst potential at fuel rich conditions (fuel entry) amounts to >1 V. When polarising a large cell to significant fuel consumption u_F (steam production), the equilibrium potential drops, for example to 0.832 V for u_F = 90%, a consumption existing locally for poorly fed anode zones. When adding to this more than 0.13 V anode overpotential loss at reasonable current densities (0.5 A/cm^2), the cathode–anode potential difference drops below 0.7 V and nickel will, thermodynamically, oxidize to NiO in these areas, with the risk of crack initiation and cell breaking. The microstructural instability towards reoxidation[6] is due to the fact that the Ni particles alter during operation (grain growth, shape change) after their reduction from the initial NiO particle framework upon first cell operation. When reoxidising, they will generally not occupy the same volumes they occupied when first fabricated.

Fig. 1 thus presents an essential feature for the mechanical reliability of anode supported SOFC where the percolating Ni network participates in the overall microstructure. As a consequence, the larger the anode overpotential loss (at given current density), the lower the thermodynamical threshold fuel utilisation (local steam concentration) will be for Ni to start reoxidizing (well below 90%). Proper flow field design for the anode chamber thus becomes paramount.

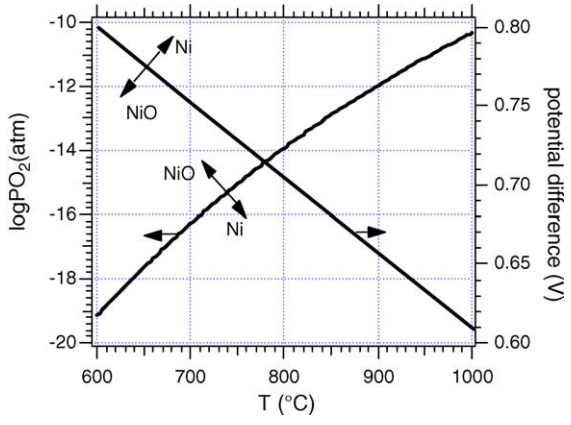

Fig. 1. Ni-NiO equilibrium as a function of temperature and oxygen partial pressure. Equivalent cathode–anode potential difference is plotted on the right hand side.

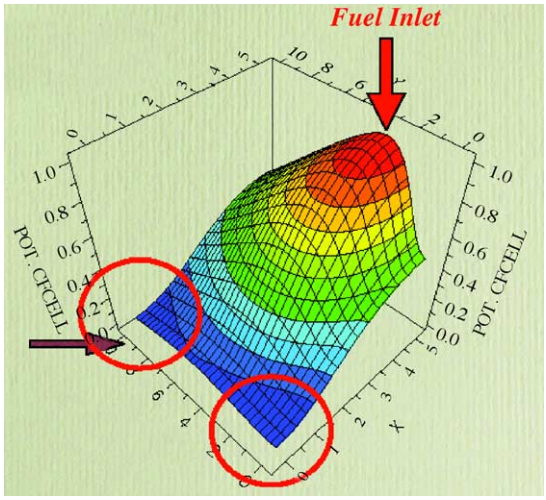

Fig. 2. Calculated H_2 fuel distribution (*z*-values compare to 97% H_2 at inlet) over a 80 mm × 80 mm cell (0.5 mm high anode chamber) with punctual inlet (upper right) and distributed outlet (lower left), having used experimental current–voltage data from a small ("button") cell to calibrate the electrochemical model. Fuel utilisation u_F 64% and total current 25.8 A (50 cm^2 active area). *X*–*Y*: cell coordinates (from fuel inlet position to outlet in *X*, full cell width in *Y*), *Z*: H_2 concentration normalised to 1.

Fig. 2 shows a numerical simulation, obtained in gPROMS environment, of the H_2 flow field over the cell configuration we use. The electrochemical model (overpotentials and resistive losses) implemented into this computation was itself calibrated on experimental data from current–voltage characteristics of small button cells.[7] Fig. 2 thus combines the electrochemical reactions with flow limitation over a larger cell of the given configuration and dimensions. The calculation is defined such that fuel conversion stops at the cell edge when the Ni reoxidation potential at the local temperature is reached: a fuel conversion of only 64% is attained (average current density of 0.516 A/cm^2) for the cell operating at 0.7 V.

Fig. 2 and higher resolution calculation for the H_2 flow field using CFD[4] shows that edge zones are especially underfed, with less than 20% H_2 locally. Whereas fuel velocity at the punctual inlet reaches 7.8 m/s, it rapidly drops to attain only 0.1 m/s in the almost stagnant corner zones (symmetrically "left" and "right" from the inlet) and 0.5 m/s at the outlet behind the (sealed) air feed hole. This was confirmed from inspection of operated cells, estimating the flow field from the coloration scale between metallic grey (fully reduced area) to light green (fully (re)oxidized area). Oxidized zones at the cell edges and behind the sealed air hole, in accordance with CFD simulation, were often observed. Frequently, cell fissures were found to depart from the (re)oxidised cell borders.

The next graphs illustrate experimental output from cells and stacks tests, relating to the flow field and anode stability just discussed.

Fig. 3 shows establishment of the open circuit voltage (OCV) on a regular 80 mm × 80 mm cell, upon first H_2

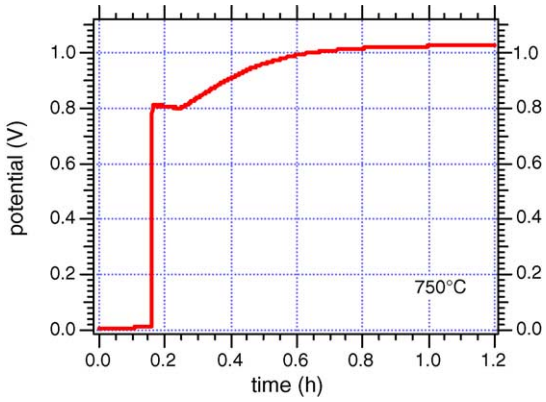

Fig. 3. Evolution of open circuit voltage of an anode support cell (80 mm × 80 mm × 0.2 mm) upon first reduction of NiO to Ni metal. H_2 flow 6 ml/min cm^2, $\lambda_{air} = 2$.

admission to the fuel inlet hole after reaching operating temperature (750 °C), while air circulates over the cathode. An immediate rise to typically 0.8 V is followed by a small drop, then a slow steady increase until stable OCV is obtained after about 1 h. This illustrates the considerable time required for the progressive reduction of NiO, contained in the initially almost dense but even thin anode (0.2 mm), to Ni metal, accompanied by steam evolution. Different OCV-time profiles as in Fig. 3 indicate different anode microstructure qualities.

Fig. 4 shows the stability behaviour of a cell galvanostatically polarised at different values. For the first 500 h, applied average current density was 0.56–0.48 A/cm^2 (u_F 50–45%), during which cell voltage was as low as 0.50–0.53 V and voltage degradation massive at a rate of −20%/1000 h. Lowering the current density to 0.36 A/cm^2 (u_F 34%), the cell operating voltage reached 0.61 V and thenceforward stabilised for over 1000 h. It seems unlikely that this strongly different behaviour would be due only to interfacial microstructural changes under the influence of a relatively limited difference in current density (0.48 A/cm^2 versus 0.36 A/cm^2). We relate the observed behaviour from Fig. 4 to the propensity of nickel anode reoxidation (hence active area loss) at lower potential (0.5 V versus 0. 6 V) and higher fuel conversion

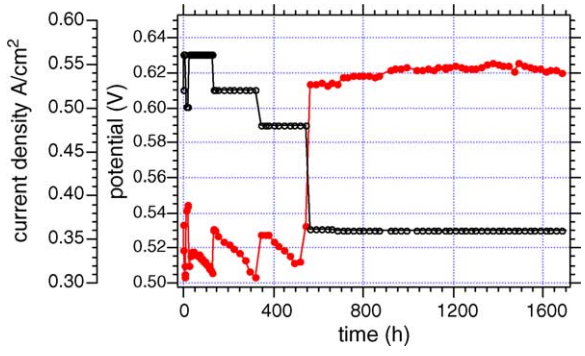

Fig. 4. Cell voltage evolution (closed circles) and applied constant current density (open circles) of an anode support cell with respect to medium term operational stability (1000–2000 h).

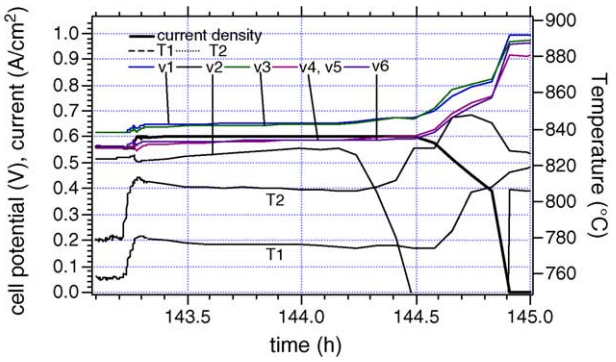

Fig. 5. Voltage evolution of 6 cells in a stack (V1–V6) polarised to 0.6 A/cm^2 (left hand side axis). Fuel utilisation 50%, $\lambda_{air} = 2$. Local temperature is plotted on the right hand side axis. The low potential of cell #2, unlike that of the other cells, is observed to change steadily before breaking down, paired with an important rise in temperature, due to direct combustion across the broken cell #2.

(surface integral 50% versus 34%) as illustrated above by Figs. 1 and 2.

Behaviour of cells in a stack is illustrated in Fig. 5. The 6-cell stack was galvanostatically polarised to 0.6 A/cm^2 (30 A total) after 143 h of operation mostly at 0.5 A/cm^2. This stack previously went through a decaying fuel supply (20 min duration, at 65 h operation, not shown) and a full thermal cycle, after which cell #2 slightly underperformed the others; its performance before these events was very similar to that of the other five cells. Damage in this cell #2 may therefore have been initiated during the supply leak or the thermal cycle. Nonetheless, total electrical power on the stack (100 W) was the same before and after the said events. At 0.6 A/cm^2 however (50% fuel utilisation), cell #2 reached a low operating point of 0.5 V, was then seen (Fig. 5) to rather steeply rise to 0.56 V (all other cell potentials between 0.58 and 0.65 V staying relatively more constant) before rapidly breaking down at 144.3 h. After current interruption the remaining cells recovered to OCV whereas cell #2 was definitely broken. The temperature indicated by two thermocouples placed just outside of the stack rose by around 30 K soon after cell #2 failed, ascribed to heating by direct combustion in the stack across the broken cell. Similar to Fig. 4, it is again demonstrated that the combination of low cell voltage (0.5 V) with even rather modest integral fuel utilisation (50%) but reasonable average current density (0.6 A/cm^2) leads to rapid degradation, up to cell cracking, most likely because of local nickel reoxidation reinforced by hot spot formation, the same current having to pass through an anode network that grows ever more resistive.

3.2. Flow distribution in stacks

Whereas the previous section centered around the flow field over one nickel anode, this section reports on the flow distribution among cells within a stack. The limitations related to Ni reoxidation and local fuel depletion remain valid in stacks, more so when total input flow is inhomogeneously distributed among cells. Moreover, proper air distribution to

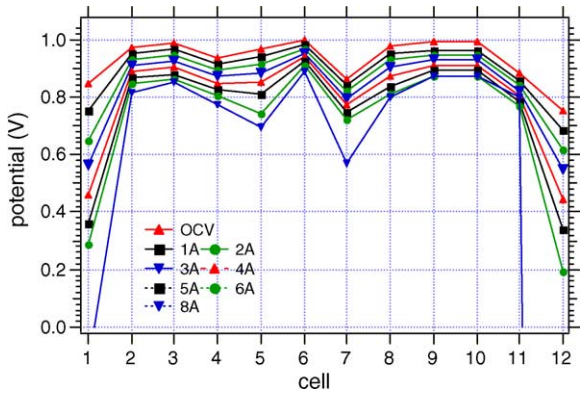

Fig. 6. Voltage on 12 cells in a stack as a function of the cell number (top to bottom). 750 °C, H_2 flow 5 ml/min cm^2, $\lambda_{air} = 1.7$.

the cathodes becomes equally vital as this flow is several times larger than that of the fuel ($2.38 \times n$ times for $\lambda_{air} = n$). Fig. 6 shows a bad case of a 12-cell stack, polarised from OCV in 1 A steps (20 mA/cm^2) to 8 A stack current. The border cells 1 and 12 are clearly limiting overall performance, breaking down in cell voltage. The middle cells 5 and 7 also tend to underperform, probably related to misalignment in stacking.

The 12-cell stack was assembled with cells of 4 mm diameter holes fed with fuel and air. Flow distribution for the cathode air tube in a 10-cell stack is calculated with FLUENT in Fig. 7. The base case (=expected flow) is 5 ml/min cm^2 for H_2 (hence 12 ml/min cm^2 air for $\lambda_{air} = 1$). Non-homogeneity in distribution is then plotted in percentage deviation from the expected flow (=1/10th of the total inlet flow) versus the cell number.

For 4 mm diameter inlet holes, and even low λ_{air} between 0.8 and 1.28 (Fig. 7a), the first and final cells receive, respectively, 25% less and 20% more than the center cells. As the experimental 12-cell stack was fed with fuel and air inlets from its top and bottom simultaneously, we therefore expect limitations on the top and bottom cells, in agreement with Figs. 6 and 7a. In addition, these cells are colder than the middle cells and more subject to mechanical constraint of the housing compressing the stack.

Fig. 7b shows the calculated flow distribution for the 10-cell stack when enlarging the feed holes to 7 mm diameter. Inhomogeneity, even for a more important air flow ($\lambda = 2.4$), now drops to maximally −8% (+7%) for the border cells. Calculations performed for 6 and 8 mm wide holes give maximal figures of −15% (+10%) and −5% (+4%), respectively. As the holes cannot be enlarged at will for mechanical reasons, a compromise of 7 mm was adopted. Importantly, pressure drops within the cells were implemented in the calculation; the values were obtained from experiment. Without this consideration, inhomogeneity would be two times worse.

A new stack of 8 cells with 7 mm feed holes was assembled and tested (feed again from top and bottom). The electrical output is plotted in Fig. 8. Homogeneity in cell performance was much improved, the spread for cells 1–7 amounting to −5% and +2.5% for lowest and best cell voltage around the average, in line with Fig. 7b. Cell 8, from a different (and

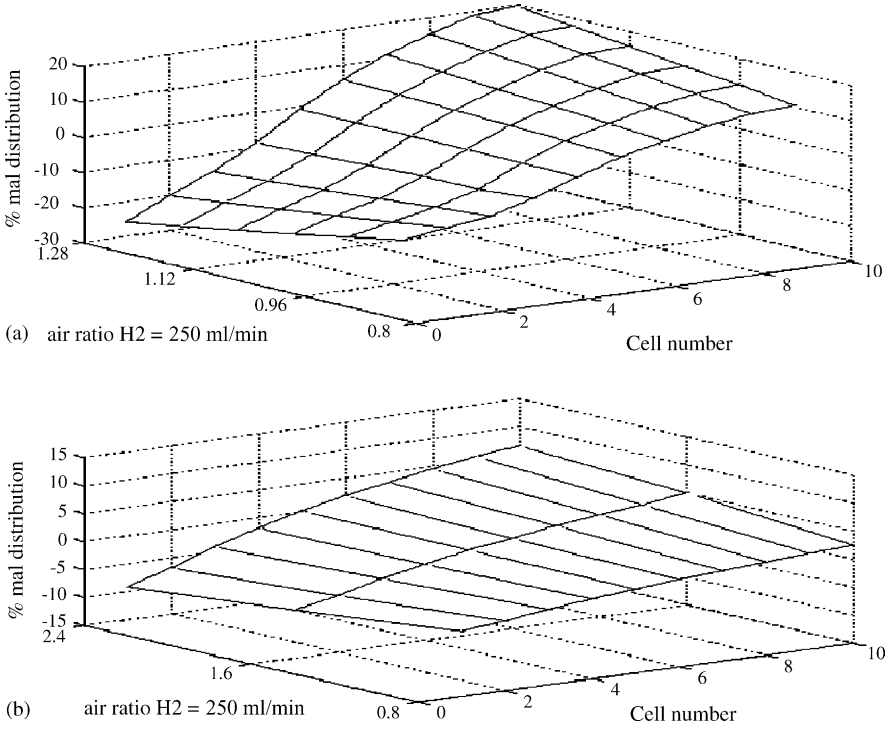

Fig. 7. Calculated air flow inhomogeneity between cells for a 10-cell stack for the configuration used here. It is expressed as percentage deviation with respect to the expected flow (=1/10th of total inlet). The top (a) presents the case of 4 mm diameter feed holes, the bottom (b) that of 7 mm diameter feed holes.

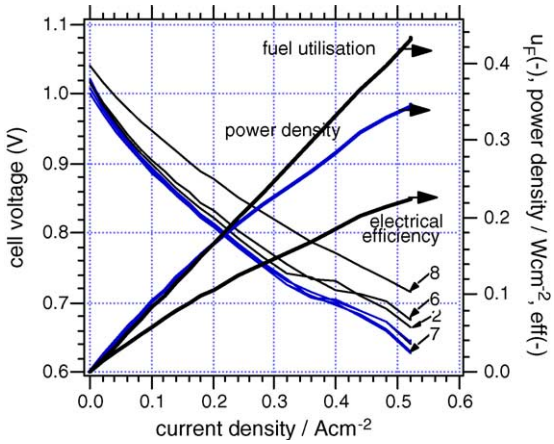

Fig. 8. Electrical output of all cells of 8-cell stack (7 mm feed holes), demonstrating acceptable performance homogeneity. 790 °C, H_2 flow 8 ml/min cm^2, $\lambda_{air} = 1.7$.

visibly superior) batch as cells 1–7 (all from the same batch), as a border cell even outperforms all others, indicating that it does not suffer from flow limitation.

3.3. Thermal gradients

Adding to nickel reoxidation and feed depletion on cells is a stress constraint due to thermal gradients, developed by the flow fields coupled with the electrochemical reactions creating a current density field on each cell. According to the formula $\sigma = \alpha \Delta T E$, with σ, stress (MPa); α, thermal expansion coefficient TEC (m/m K) and E, Young modulus (GPa); the allowable gradient ΔT can be estimated when the averaged TEC ($12.8–13.1 \times 10^{-6}$ m/m K for our anode supports, experimental value), rupture limit and Young modulus are known. In the case of 8YSZ electrolyte supported cells (TEC = 10×10^{-6} m/m K), $E = 200$ GPa and $\sigma = 200$ MPa, giving allowable gradients of 100 K. For Ni-8YSZ composite anode supports, the tolerable gradient lies expectantly lower. The temperature field was calculated by CFD with FLUENT. For an average case (0.6 V, u_F 40%, 19 A, inlet 750 °C), the hottest zones (870 °C) appear symmetrically left and right from the fuel entry and the coldest zone behind the (sealed) air hole (760 °C). At the distributed fuel exit behind the air hole, post-combustion of unused fuel with surrounding air takes place. This area is thus very critical as steep thermal gradients occur. In addition, it is vulnerable to reoxidation since not well flooded with fuel (Fig. 2).

The current density field for a case with appreciable total current (0.7 V, u_F 60%, 28.8 A, average 0.58 A/cm^2), Fig. 9, shows local values of 1 A/cm^2 at the fuel inlet down to 0.4 A/cm^2 towards the corners. This is compared with experimental values of local current density, measured on a segmented cell of the same geometry. Details on this experiment will be published in near future. Fig. 10 gives the measured local current density values for the cell, compartmented in eight segments as shown, with respect to the fuel

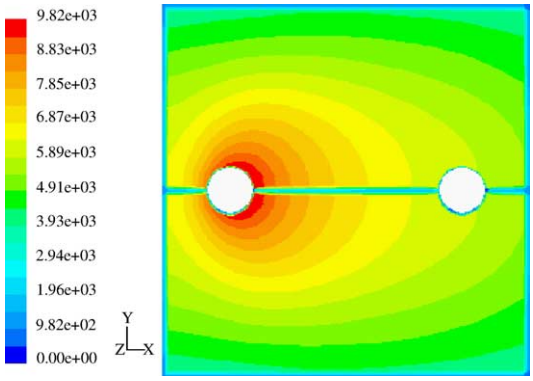

Fig. 9. Calculated current density field (0.7 V, u_F 60%, 28.8 A), expressed in A/m^2, for anode support cell (80 mm × 80 mm × 0.2 mm) fed with H_2 (7 ml/min cm^2) and air ($\lambda = 2$).

entry segment set equal to 100% (ca. 1 A/cm^2). In spite of the unexpected asymmetry (due to contact imperfections in the experimental assembly), the comparison with the numerical results (Fig. 9) well respects the tendencies, to a certain extent also quantitatively.

The fuel cell engineer wishes eventually to achieve highest power density for the lowest possible thermal gradients. This challenge calls for a simultaneous consideration and optimisation of the two conflicting parameters. This type of calculation has been developed,[8] with multi-objective optimisation using a genetic algorithm to generate and select best solution populations to the stated problem, and is now being applied to our anode supported fuel cell stacking.

The degrees of freedom are the operating conditions (temperature, excess air, fuel flow) and the cell geometry (area, shape, pressure drop, thermal conductivity of current

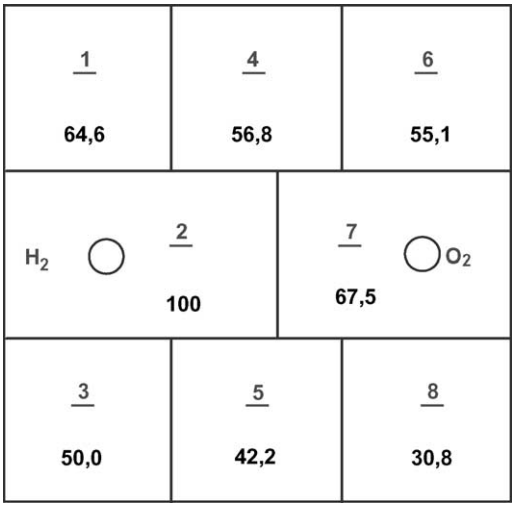

Fig. 10. Measured local current density (average 0.18 A/cm^2, u_F 35%, 0.75 V) expressed in percentage with respect to the fuel inlet segment (H_2, 100%) on a segmented cell (8 compartments) of the same geometry as the other anode support cells reported here.

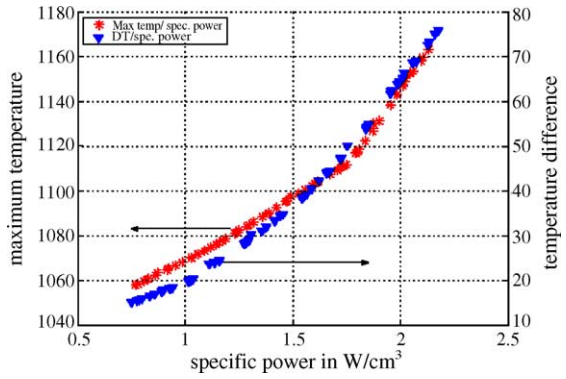

Fig. 11. Optimal solution points for the studied anode supported fuel cell stacks when pursuing maximal volumetric power density (W/ml) and minimal thermal gradient (ΔT) or lowest hottest cell temperature (T_{max}).

collector). The objectives are the volumetric power density (W/ml) and thermal gradient (ΔT) or maximum temperature (T_{max}) on a cell. A first result is given in Fig. 11 as a pareto-curve, uniting all optimal solutions for joint objective pairs. Our present experimental result is a stack power density of 1 W/ml for thermal gradients around 80 K. Fig. 11 thus indicates an important improvement potential: for the same 1 W/ml power density, the thermal gradient could optimally be reduced to 20 K, and for a same 80 K thermal gradient, an optimal power density of >2 W/ml would be achievable.

4. Conclusion

Experimental results on Ni-zirconia anode supported fuel cells in a particular stack configuration (750–800 °C, 50 cm^2 active area, limited flows (H_2, air), punctual internal manifolds, metal current collectors) were presented. Limitations were observed in terms of fuel utilisation (50%), of non-homogeneous cell performance in stacks, and of stability both electrochemical (voltage degradation) and mechanical (cell break down). These results were confronted with theoretical and modeling aspects, demonstrating the critical issues of nickel reoxidation in the anode support, of anode and cathode flow fields within both cells and stacks, and of thermal gradients coupled to the current density field. In follow-up experiments, the modeling results (i) on the one hand have led to improved behaviour, such as medium term stability (1000–2000 h) and flow distribution in stacks (feed hole enlargement), and (ii) on the other hand could be validated (local current density measurement). Multi-objective optimisation shows the way to better cell and stack configuration, which is now under further experimental development.

Acknowledgements

Financial support is gratefully acknowledged from the Swiss Commission for Technology and Innovation (CTI 6649.3 IWS-IW) and the Swiss Federal Energy Office (OFEN 86-895, 86-755). Thanks are due to colleagues from HTceramix Inc., Switzerland, for fabrication and supply of fuel cells and stacks, to J. Sfeir (EMPA, Switzerland, Fig. 1) and F. Ravussin (EPFL, Fig. 10).

References

1. Steinberger-Wilckens, R., de Haart, L. G. J., Vincke, I. C., Blum, L., Cramer, A., Remmel, J. *et al.*, Recent results of stack development at Forschungszentrum Juelich. In *Proceedings of the 8th International Symposium on Solid Oxide Fuel Cells*, ed. S. Singhal and M. Dokiya, April 2003, pp. 98–104.
2. Van herle, J., Ihringer, R., Vasquez, R., Constantin, L. and Bucheli, O., Anode supported SOFC with screen-printed cathodes. *J. Eur. Ceram. Soc.*, 2001, **21**, 1855–1859.
3. Molinelli, M., Larrain, D., Ihringer, R., Constantin, L., Autissier, N., Bucheli, O. *et al.*, Current collection and stacking of anode support cells with metal interconnects to compact repeating units. In *Proceedings of the 8th International Symposium on Solid Oxide Fuel Cells*, ed. S. Singhal and M. Dokiya, April 2003, pp. 905–913.
4. Autissier, N., Larrain, D., Van herle, J. and Favrat, D., CFD simulation tool for SOFC. *J. Power Sources*, 2004, **131**, 313–319.
5. Oh, M. and Pantelides, C., A modeling and simulation language for combined lumped and distributed parameters systems. *Comput. Chem. Eng.*, 1996, **20**(6/7), 611–633.
6. Tiketar, N., Armstrong, T. and Virkar, A., Reduction and reoxidation kinetics of nickel-based SOFC anodes. In *Proceedings of the 8th International Symposium on Solid Oxide Fuel Cells*, ed. S. Singhal and M. Dokiya, April 2003, pp. 670–679.
7. Larrain, D., Van herle, J., MarŽchal, F. and Favrat, D., Thermal modeling of a small anode supported solid oxide fuel cell. *J. Power Sources*, 2003, **118**, 367–374.
8. Larrain, D., Van herle, J., MarŽchal, F. and Favrat, D., Generalized model of SOFC planar repeat element for design optimisation. *J. Power Sources*, 2004, **131**, 304–312.